ELSEVIER

Journal of Hazardous Materials 41 (1995) 47–64

JOURNAL OF HAZARDOUS MATERIALS

The reaction kinetics, decomposition pathways and intermediate formations of phenol in ozonation, UV/O_3 and UV/H_2O_2 processes

Ching-Rong Huang*, Hung-Yee Shu

Department of Chemical Engineering, Chemistry and Environmental Science, New Jersey Institute of Technology, Newark, NJ 07102, USA

Received 9 March 1994; accepted in revised form 4 October 1994

Abstract

Recently, advanced oxidation processes (AOPs) have been developed as an emerging technology for treating hazardous organics treatment in wastewater and groundwater. In this paper, the phenol decomposition pathways and intermediates in ozonation and two AOPs (e.g. UV/ozone, UV/hydrogen peroxide) were studied in a photochemical pilot reactor utilizing 5000 W low-pressure mercury lamp. It was observed that, in the UV/hydrogen peroxide system, phenol was first oxidized by hydroxyl radical into hydroquinone and catechol which finally decomposed into organic acids and carbon dioxide. Additionally, some other higher molecular weight products such as 4-phenoxy phenol, 2,2-dimethoxyethyl benzene, α-methoxy-α-methyl benzeneethanol, etc. were also produced. However, in the ozonation process phenol was oxidized into hydroquinone and catechol which were degraded into acids and carbon dioxide without high molecular weight byproducts. In the UV/ozone process, the major reaction pathway was similar to that of ozonation, but some 4-phenoxy phenol was formed and decomposed ultimately.

1. Introduction

Industrial process plants generating wastewater containing organic pollutants are required to pretreat their wastes before discharging into POTWs (publicly owned treatment works). Goronszy et al. [1] suggested chemical oxidation as the most effective and simplest pretreatment for organics. This process utilizes oxidants (such as chlorine, ozone, hydrogen peroxide, potassium permanganate and chlorine dioxide, etc.) to destroy the odor-causing sulfur compounds, control bacterial growth, and reduce COD (chemical oxygen demand).

* Corresponding author.

SSDI 0304-3894(94)00093-X

Ozone and hydrogen peroxide have been employed as oxidants in many water and wastewater treatment applications. Theoretically, ozone and hydrogen peroxide should be able to oxidize inorganics to their higher oxidation states while oxidizing organic compounds into carbon dioxide and water. However, for the refractory organics in water, ozone or hydrogen peroxide alone without UV radiation reactions exhibited limited selections and lower reaction rates, the AOPs were developed. The UV-induced advanced oxidation processes (AOPs) generally utilize ultraviolet (UV) radiation with ozone (O_3) or hydrogen peroxide (H_2O_2) to generate hydroxyl radicals; this process can achieve complete destruction of organic contaminants [1]. Although the UV/ozone process was undoubtedly effective with many refractory organics, there were some drawbacks. First, ozone is an unstable gas which must be generated and used on-site immediately. Second, an ozone-water contacting device which can adequately transfer ozone into the liquid phase must be provided. However, hydrogen peroxide which was easier to be stored and transported may oxidize the organics as well as ozone does. These advantages make the UV/hydrogen peroxide process more attractive to the researchers.

The UV/hydrogen peroxide system has proved to be effective for the treatment of water contaminated with refractory compounds such as nitrosamines, various halogenated aliphatics, aromatic organics (benzene, toluene, chlorobenzene, phenol, chlorophenols, dimethyl phthalate and diethyl phthalate, etc.), 2,4-dinitrotoluene (explosive from military munition facilities), groundwater contaminated with TCE (tri-chloroethylene), 1,1-DCA (1,1-dichloroethane), 1,1,1-TCA (1,1,1-trichloroethane), and chemicals from paper industry [2–8]. Among all the operational parameters, the UV transmittance in wastewater (because it affects the treatment effectiveness) was considered as an important variable for all the UV oxidation processes. Transmittance to wastewater is reduced by turbidity, colored organic and inorganic compounds in the wastewater. The local light intensity decreases exponentially when the wastewater transmittance to wastewater is decreases. Extremely low transmittance could make the photo-oxidation process very expensive and impractical [9]. Therefore, UV transmittance should play an important role in the modeling work of a UV-induced AOP reactor.

Phenol is generally found in the wastewater of various industries such as the dye, epoxy resins, additives and aromatic chemical, solvents and pharmaceutical industries. It is generated at a rate of 2200 to 589,230 lbs annually per individual factory [10]. Therefore, it is important to study the destruction of phenol and could especially improve the understanding for the degradations of its derivatives like chlorophenols, chlorinated pesticides, phenoxy herbicides, etc. However the chemical kinetics, formation of intermediates and decomposition pathways of phenol in the UV/O_3, UV/H_2O_2, and ozonation processes have not been delineated yet. Some previous fundamental research in similar AOPs has focused on the formation of intermediates which can be used as a comparison for our study.

The heterogeneous photocatalytic oxidation of phenol in water by UV-induced oxidation on TiO_2 particles was reported by Trillas et al. [11] and Wei et al. [12]. Intermediates detected were hydroquinone, paraquinone, and 1,2,4-benzenetriol. These reports suggested the lower the initial phenol concentrations, the higher the

degradation rates approached. Similarly, Al-Hayek et al. oxidized phenol in water using hydrogen peroxide on alumina-supported iron. He obtained the pyrocatechol, hydroquinone, and *p*-benzoquinone as the intermediates [13]. Another process, supercritical fluid oxidation, was also utilized to oxidize phenol in water [14–16]. In this process, Thornton et al. studied the pathways and reaction kinetics of phenol oxidation in supercritical water. The byproducts were also identified as polycyclic compounds such as 2- and 4-phenoxyphenol, 2,2′-biphenol, and dibenzofuran. They observed that the empirical degradation rate was proportional to the phenol concentration to 0.5 power of the oxygen concentration and to 0.7 power of the water concentration. The elementary reaction rates of phenol with hydroxyl radicals were reported by Field et al. as 4.5×10^9 l/gmol/s for addition reactions and 2.1×10^9 l/gmol s for abstraction reactions [17].

The objective of this study was to identify the reaction kinetics, pathways and intermediates of phenol degradation under ozonation, UV/hydrogen peroxide, and UV/ozone processes. Using a pilot-scale reactor, scale-up parameters such as rate constants, mass transfer coefficients were obtained. The intermediates were identified by GC/MS. Ultimately, the mathematical modeling predictions of reaction kinetics provided excellent agreement with experimental data.

2. Proposed model

2.1. Light intensity model

Light intensity which affects the decomposition rate in an AOP reactor was an important parameter for our reactor modeling. Radial approximation of the infinite line source model could be described as follows: the light intensity, I, at any point p in the reactor was related to the surface flux, I_0, by a one-dimension form of Lambert's law of absorption, where E was the monochromatic absorbance of water.

$$\frac{1}{r}\frac{\mathrm{d}(rI)}{\mathrm{d}r} = -EI.$$

The above equation was integrated using a boundary condition of $I = I_0$ when $r = r_0$ and a definition of the ratio (the average point intensity to the surface flux at the quartz tube in the reactor) as the intensity factor, m. Here, R denoted reactor radius, r_0 was the radius of the lamp with quartz shell, $\bar{I}$ denoted average point intensity. The result was

$$m = \frac{\bar{I}}{I_0} = \frac{2r_0}{E(R^2 - r_0^2)}[1 - \mathrm{e}^{-E(R-r_0)}].$$

2.2. Free radical reactions

In order to estimate the decomposition rates of specific chemicals which reacted with OH· and HO_2·, some reaction rate constants were obtained from the literature

Table 1
Rate constants of some important reactions (l/gmol s)

Reactions	Rate constants	Researchers
$H_2O_2 + OH\cdot \xrightarrow{k_{10}} HO_2\cdot + H_2O$	$k_{10} = 2.7 \times 10^7$	Christense (1982)
$H_2O_2 + HO_2\cdot \xrightarrow{k_{11}} OH\cdot + H_2O + O_2$	$k_{11} = 3.7$	Koppenol (1978)
$2OH\cdot \xrightarrow{k_{14}} H_2O_2$	$k_{14} = 4.0 \times 10^9$	Thomas (1965)
$2HO_2\cdot \xrightarrow{k_{15}} H_2O_2 + O_2$	$k_{15} = 8.3 \times 10^5$	Beilski (1978)
$OH\cdot + HO_2\cdot \xrightarrow{k_{16}} H_2O + O_2$	$k_{16} = 3.7 \times 10^{10}$	Burrows (1981)
$OH\cdot + O_3 \xrightarrow{k_8} O_2 + HO_2\cdot$	$k_8 = 1.1 \times 10^8$	Sehested (1982)

[18–20] and tabulated in Table 1. As a result, the reaction rate constants of hydrogen peroxide induced by UV radiation could be solved numerically.

2.3. Ozonation of phenol

Ozone can decompose many organic pollutants in water. Therefore, the ozonation system was designed to measure the effects of ozone on the decomposition. From our literature review, we found that ozone initially decomposes to hydroxyl radicals. Hydroxyl radicals then attack the pollutants in water and produced hydroperoxide radicals which can also oxidize pollutants. There is a fairly high concentration of aqueous ozone relative to the hydroxyl radical concentration. There also is a fast reaction between ozone and phenol. The relative rates for ozone dissociation in water and the hydroxyl radical production were slower than that of the ozonation of phenol. Therefore, we proposed the mechanism of phenol ozonation could be simplified to ozone mass transfer:

$$O_{3g} \xrightarrow{K_{LO_3}a} O_{3_L},$$

reaction of ozone and phenol:

$$\text{phenol} + O_3 \xrightarrow{k_1} \text{decomposed products.}$$

2.4. Reaction with hydrogen peroxide and UV light

Hydrogen peroxide served as one source of hydroxyl radical in aqueous solution under UV radiation. Also, phenol reacted with hydrogen peroxide by UV radiation

could be a fundamental understanding that of the UV/ozone process. The following eight major chemical reactions are often quoted by different authors in a UV/hydrogen peroxide system. The first six are reactions between free radicals and hydrogen peroxide; the last two reactions are pathways of phenol decomposition.

$$H_2O_2 + h\nu \xrightarrow{K_{IH_2O_2}I} 2OH\cdot$$

$$H_2O_2 + OH\cdot \xrightarrow{k_{10}} HO_2\cdot + H_2O,$$

$$H_2O_2 + HO_2\cdot \xrightarrow{k_{11}} OH\cdot + H_2O + O_2,$$

$$2OH\cdot \xrightarrow{k_{14}} H_2O_2,$$

$$2HO_2\cdot \xrightarrow{k_{15}} H_2O_2 + O_2,$$

$$OH\cdot + HO_2\cdot \xrightarrow{k_{16}} H_2O + O_2,$$

$$\text{phenol} + OH\cdot \xrightarrow{k_4} \text{decomposed products}$$

$$\text{phenol} + HO_2\cdot \xrightarrow{k_5} \text{decomposed products.}$$

2.5. *Reaction with ozone and UV light*

Ozone in aqueous solution will generate hydroxyl free radicals under UV radiation. Simultaneous reactions and ozone mass transfer including the first ten equations below will proceed immediately. The three last reactions are major pathway of phenol decomposition used in our kinetic model.

$$O_{3_g} \xrightarrow{K_{LO_3}a} O_{3_l},$$

$$O_3 + H_2O + h\nu \xrightarrow{K_{IO_3}I} O_2 + 2OH\cdot,$$

$$O_3 + OH\cdot \xrightarrow{k_8} HO_2\cdot + O_2,$$

$$O_3 + HO_2\cdot \xrightarrow{k_{12}} OH\cdot + 2O_2,$$

$$H_2O_2 + h\nu \xrightarrow{k_{IH_2O_2}I} 2OH\cdot,$$

$$H_2O_2 + OH\cdot \xrightarrow{k_{10}} HO_2\cdot + H_2O,$$

$$H_2O_2 + HO_2\cdot \xrightarrow{k_{11}} OH\cdot + H_2O + O_2,$$

$$2OH\cdot \xrightarrow{k_{14}} H_2O_2,$$

$$2HO_2\cdot \xrightarrow{k_{15}} H_2O_2 + O_2,$$

$$OH\cdot + HO_2\cdot \xrightarrow{k_{16}} H_2O + O_2,$$

$$\text{phenol} + O_3 \xrightarrow{k_1} \text{decomposed products},$$

$$\text{phenol} + OH\cdot \xrightarrow{k_4} \text{decomposed products},$$

$$\text{phenol} + HO_2\cdot \xrightarrow{k_5} \text{decomposed products}.$$

3. Experimental

3.1. Materials

Hydrogen peroxide (30% w/w) was obtained from Fluka Chemical Co. Phenol, catechol and hydroquinone were obtained from Aldrich Chemical Co. and used without further purification. HPLC solvents (acetonitrile and acetic acid) were HPLC grade, the reagents for the hydrogen peroxide measurements were all ACS analytical reagent grade from Fisher Scientific Co. The stock solutions were refrigerated and stored in the dark.

The Welsbach T-816 ozone generator, from the Welsbach Ozone System Corporation, Philadelphia, PA, could produce a minimum of 16 g of pure, dry ozone per hour. This unit was a corona discharge-type ozone generator cooled by water. The ozone output flow rates were adjustable by a ball valve from 4.5 to 9.0 l/min. Pure (99.6%) dry oxygen was utilized for ozone generation in this operation.

3.2. Apparatus

The phenol solution was photo-decomposed in a stainless steel reactor, 33 cm diameter, 150 cm height, with a 100 l holdup volume. A Canrad Hanovia low-pressure

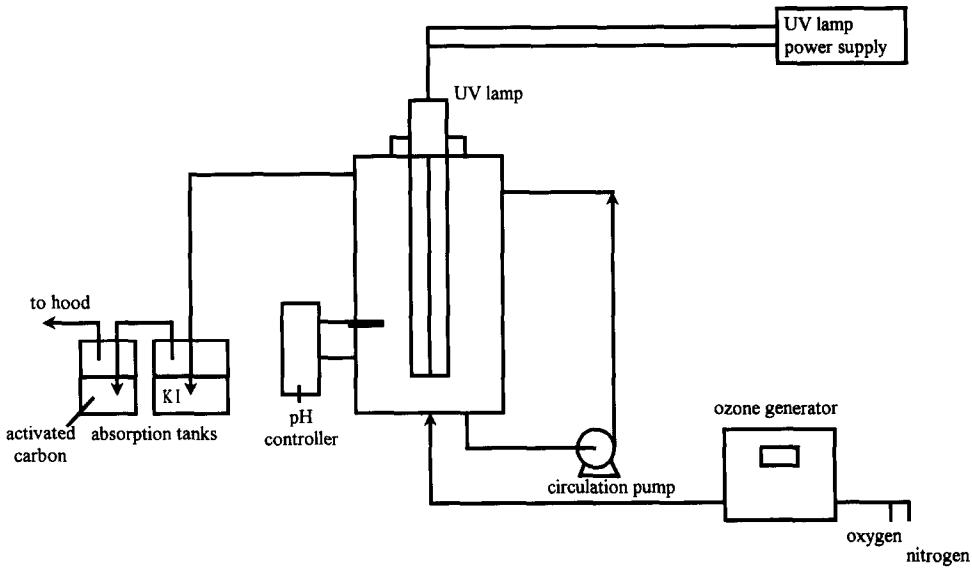

Fig. 1. Schematic diagram of the apparatus used to study the ozonation and advanced oxidation processes including UV/ozone and UV/hydrogen peroxide.

mercury lamp, with 25 in. arc length and 5000 W output, was located at the reactor center. The lamp was protected by two wells: one well contained nitrogen gas to avoid explosive hazard, and the other one was used for cooling water circulation. Complete mixing of the solution could be obtained by pumped recycle solution and plus nitrogen bubbled from the reactor bottom. However, in the ozonation tests, ozone was bubbled through the sparger at the reactor bottom. The pH was monitored by a pH controller and monitor. The reactor could be run as a batch or continuous stirred tank reactor (CSTR). The off-gas was passed through an activated carbon adsorption column to prevent volatile organic emissions into the laboratory. The schematic diagram of the apparatus is shown in Fig. 1.

3.3. Analyses

To determine the phenol concentrations and reaction intermediates, a Waters 600E system controller with a Waters 715 Ultra Wisp Sample Processor and Waters 994 programmable photodiode array detector coupled with a Chromatography server data acquiring system was employed. The stationary phase was Nova-Pak 3.9 mm × 150 mm, C_{18} column. The mobile phase was 70% of 1% acetic acid in water and 30% of 1% acetic acid in acetonitrile

The hydrogen peroxide concentration was determined by the spectrophotometric method proposed by Masschelein et al. [21]. They suggested one add Co(II) reagent

and hexametaphosphate solution to an 80 ml sample, and make up to 100 ml with saturated bicarbonate solution. A green color is developed and can be measured at 260 nm. Then, measured absorbances was compared with calibration curve to calculate the exact hydrogen peroxide concentrations.

The aqueous ozone concentration measurements were made using the iodometric method which Shechter [22] proposed. First, one adds a 5-ml sample solution to a vial containing 5 ml 2% solution (by dissolving 13.61 g potassium dihydrogenphosphate, 14.2 g anhydrous disodium hydrogen phosphate and 20.0 g potassium iodide in 1000 ml distilled water) immediately after withdrawing from reactor. Thirty minutes later, one measures the absorbance at 352 nm using a spectrophotometer and compares with the calibration curve to calculate the ozone concentrations.

An HP 5890 series II gas chromatograph (GC) with HP 5988A mass spectrometry (MS) detector and Pascal Chem Station data system was employed to identify the oxidation intermediates. The column was a 25 m × 0.25 mm ID, methyl silicon cross-link capillary column. The temperature was programmed from 60 °C for 1 min to 200 °C for 5 min with increasing rate of 8 °C/min. The intermediates were collected and extracted, concentrated by SPE (solid phase extraction) tubes, subsequently injected into GC/MS. SPE tubes were preconditioned with 2 ml methanol and 2 ml water and 400 ml sample was passed through the SPE tube by applying vacuum. Finally, elute the organics by 2 ml methanol. The eluted solutions were collected and analyzed by GC/MS.

4. Results and discussion

4.1. Mass transfer and photo-decomposition of ozone in aqueous phase

The volumetric mass transfer coefficient ($K_{LO_3}a$) and the saturation concentration (C_{SO_3}) of ozone in the sparged reactor could be measured by bubbling ozone into the reactor. Fig. 2 is a plot of the ozone concentration in the aqueous phase versus the time with different gas phase ozone concentrations.

The gas phase ozone concentration was controlled by the flow rate of oxygen to the ozone generator. The higher flow rate of oxygen gas gave a less concentrated ozone feed shear. First, ozone was sparged into the aqueous phase reaching saturation concentration (C_{SO_3}) in 15 min. Thereafter, ozone was continuously bubbled into the reactor to keep a stable ozone concentration in the liquid phase. After 48 min of sparging, while the UV lamp was turned on, the photodecomposition of ozone was started to decompose ozone and generate the free radicals; then the ozone concentration dropped rapidly. Fig. 2 consist of two segments, the first segment was the unsteady-state mass transfer of ozone to the aqueous phase and the second segment was the decomposition of ozone in the aqueous after the UV lamp was turned on at time of 48 min. From these experimental data, the values of mass transfer coefficient ($K_{LO_3}a$), photodecomposition rate constant of aqueous ozone ($k_{IO_3}I$) and saturated concentration of ozone (C_{SO_3}) in water were obtained and tabulated in Table 2 using

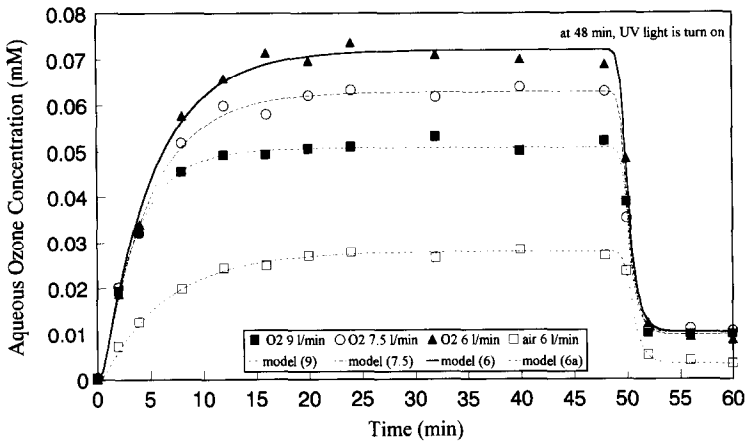

Fig. 2. Plot of data for ozone mass transfer rate under different oxygen and air flow rate; at $t = 48$ min UV lamp was turned on and ozone concentration decreased.

Table 2
Mass transfer coefficient, saturated concentration and photodecomposition rate constant for ozone in the photochemical reactor

Oxygen source	$K_{LO_3}a$ (s^{-1})	C_{SO_3} (mM)	$K_{LO_3}a \times C_{SO_3}$ (mM/s)	$k_{IO_3}I$ (s^{-1})
Oxygen 9.0 l/min	5.080×10^{-3}	0.0508	0.258×10^{-3}	0.145
Oxygen 7.5 l/min	3.702×10^{-3}	0.0628	0.232×10^{-3}	0.145
Oxygen 6.0 l/min	3.387×10^{-3}	0.0720	0.244×10^{-3}	0.145
Air 6.0 l/min	2.775×10^{-3}	0.0279	0.774×10^{-4}	0.145

the following equations:

$$\frac{dC_{O_3}}{dt} = K_{LO_3}a \times (C_{SO_3} - C_{O_3}),$$

$$K_{LO_3}a \times (C_{SO_3} - C_{O_3}) \approx k_{IO_3}I \times C_{O_3}.$$

Here, C_{O_3} denotes the ozone concentration at any time t. The aqeous saturated ozone concentrations C_{SO_3} could be obtained by reading the steady-state value of ozone concentrations from the experimental runs. The mass transfer coefficients, $K_{LO_3}a$, were calculated by fitting the experimental ozone concentration curve respected to time to the above equation.

Results in Table 2 indicated that the higher the oxygen flow rate through ozone generator (with low gaseous ozone concentration) the larger the mass transfer coefficient was, but it simultaneously yielded a lower saturated ozone concentration as

a result of a lower gas phase ozone concentration. However, the initial mass transfer rate which was the product of mass transfer coefficient and saturated concentration ($K_{LO_3}a \times C_{SO_3}$) in column 4 for the first three cases was very close to the same value. It may be concluded that the effect of increasing the mass transfer area compensated for the effect of ozone gas concentration decrease. Also in Table 2, column 5 reports the photo-decomposition rate constant, $k_{IO_3}I$, calculated from the second portion of Fig. 2. It has been reported in the literature that the decomposition of ozone under UV radiation is very fast. But the quantitative value of the rate constant was not known. Using our model to fit all four sets of data, a value of $k_{IO_3}I$ was calculated as $0.145\ s^{-1}$.

4.2. Decomposition of hydrogen peroxide under UV radiation

The hydrogen peroxide decomposition under UV radiation was a fundamental investigation which may lead to better comprehension of the AOPs' reaction mechanisms. Data for hydrogen peroxide decomposition under UV irradiation was plotted in Fig. 3 with three different initial hydrogen peroxide concentration of 7.081, 4.736, and 2.572 mM (adding 60, 40 and 20 ml of 35% hydrogen peroxide solution to 100 liters deionized water). The calculated photodecomposition rate constants of hydrogen peroxide, $k_{IH_2O_2}I$, are tabulated in conformance with Table 3. The kinetic model included photodecomposition of hydrogen peroxide and the reactions listed in Table 1. The hydrogen peroxide concentration during the reaction could be calculated by mass balance as follows:

$$\frac{dC_{H_2O_2}}{dt} = -k_{IH_2O_2}IC_{H_2O_2} - k_{10}C_{H_2O_2}C_{OH} - k_{11}C_{H_2O_2}C_{HO_2\cdot} + k_{14}C^2_{OH\cdot} + k_{15}C^2_{HO_2\cdot}$$

$$\frac{dC_{OH\cdot}}{dt} = 2k_{IH_2O_2}IC_{H_2O_2} - k_{10}C_{H_2O_2}C_{OH\cdot} + k_{11}C_{H_2O_2}C_{HO_2\cdot} - 2k_{14}C^2_{OH\cdot} - k_{16}C_{OH\cdot}C_{HO_2\cdot}$$

$$\frac{dC_{HO_2\cdot}}{dt} = k_{10}C_{H_2O_2}C_{OH\cdot} - k_{11}C_{H_2O_2}C_{HO_2\cdot} - 2k_{15}C^2_{HO_2\cdot} - k_{16}C_{OH\cdot}C_{HO_2\cdot}.$$

The photodecomposition rate constants of hydrogen peroxide were approximated by fitting the experimental data into the model which was modified several times to make better predictions. In the first instance, it was assumed that the hydrogen peroxide solution did not absorb UV light and gas bubble volume was neglected ($k_{IH_2O_2}I = k_{IH_2O_2}I_0$). Under these assumptions, there were three different photodecomposition rate constants for three initial concentrations of H_2O_2.

In the second instance, the UV light absorbed by the hydrogen peroxide solution was considered and the light intensity was assumed to decay exponentially as a function of radial distance following Lambert's law as described in "Proposed Model" section ($k_{IH_2O2}I = k_{IH_2O_2}I_0 \times m$), but the gas bubble volume was neglected.

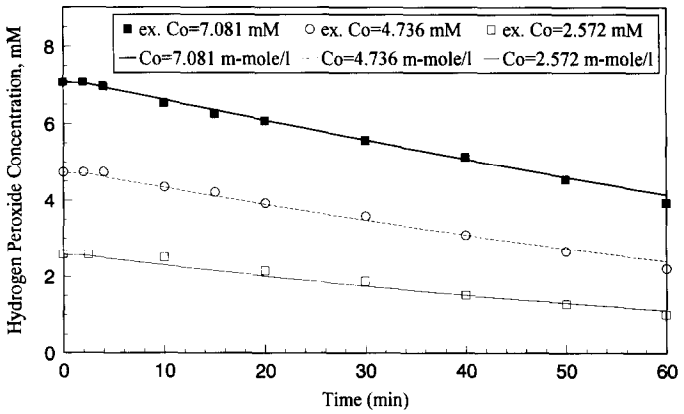

Fig. 3. Plot of hydrogen peroxide decomposition under UV radiation and model fitting, hydrogen peroxide concentration from 2.57 to 7.08 mg mol/l.

Table 3
Photodecomposition rate constants ($k_{lH_2O_2}I_0$, s^{-1}) of hydrogen peroxide at the UV lamp wall in three steps of modification

	Initial H_2O_2 concentration		
	7.081 m*M*	4.736 m*M*	2.572 m*M*
Original model	0.521×10^{-3}	0.669×10^{-3}	0.778×10^{-3}
1st modification	0.943×10^{-3}	0.864×10^{-3}	0.780×10^{-3}
2nd modification	1.091×10^{-3}	1.080×10^{-3}	1.080×10^{-3}

Under these assumptions, the model again yielded three different decomposition rate constants at the lamp wall.

Finally, under the conditions where the UV light absorbed by the hydrogen peroxide solution and the gas bubble volume were taken into account, only one decomposition rate was obtained for the three determinations. Therefore, this model was accepted as the best model to express the mechanism of hydrogen peroxide photo-oxidation based on the consistent agreement between experimental data and model predictions. Given the last modification, the three rate constants of photodecomposition of hydrogen peroxide were independent of inital hydrogen peroxide concentration and closed to a unique value of $k_{lH_2O_2}I_0 = 1.085 \pm 0.055 \times 10^{-3}\ s^{-1}$. By comparison of the photodecomposition of hydrogen peroxide and ozone under UV irradiation, the decomposition rate constant of ozone was approximately 150 times larger than the one for hydrogen peroxide.

4.3. Ozonation of phenol

The mechanism of phenol decomposition by ozonation was given in Fig. 4. Experimental and modeling data were plotted in Fig. 6 and the GC/MS total ion

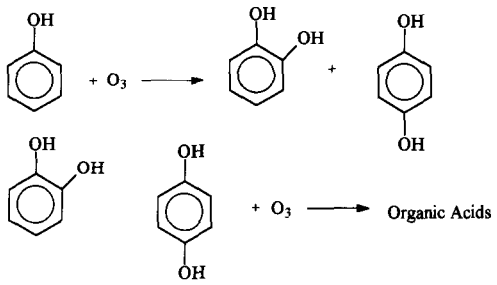

Proposed reaction pathway of phenol decomposition by ozonation

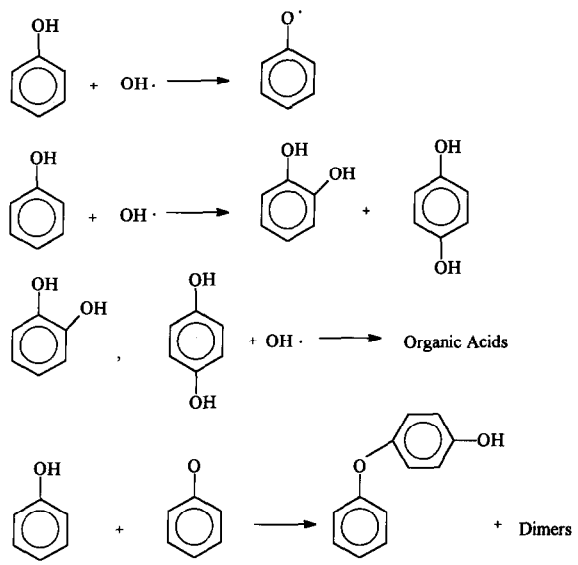

Proposed reaction pathway of phenol decomposition by hydroxyl radicals

Fig. 4. Proposed reaction pathways for ozonation, UV/hydrogen peroxide and UV/ozone systems.

chromatograph for 24 min of reaction time was shown in Fig. 5. The calculated rate constant of formation of intermediates, hydroquinone and catechol, from data in Fig. 6 is 1.30×10^3 l/mol s. Also, the major intermediates were hydroquinone and catechol. However, a small quantity of α-methoxy-α-methyl benzeneethanol was found as an intermediate in GC/MS chromatograph.

4.4. Photolytic hydrogen peroxide oxidation

The possible decomposition mechanisms of phenol by UV radiation and hydrogen peroxide were suggested as in Fig. 4. From GC/MS analysis, different oxidation

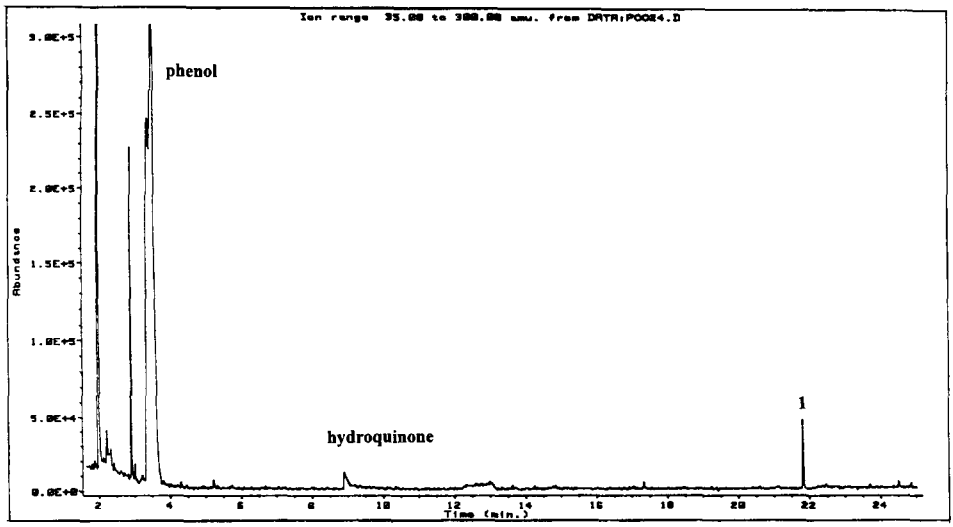

Fig. 5. GC/MS total ion chromatograph for phenol decomposition by ozonation after 24 min of reaction. Intermediate marked No. 1 is α-methoxy-α-methyl-benzeneethanol.

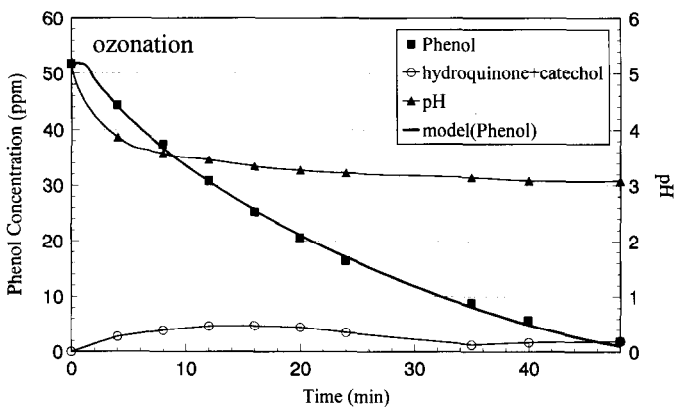

Fig. 6. Experimental data and model fitting for phenol decomposition by ozonation. Initial phenol concentration is 52.2 ppm; the oxygen flow rate to the ozone generator was 6.0 l/min oxygen.

products were observed for UV/hydrogen peroxide oxidation. Catechol and hydroquinone were the major intermediates. Meanwhile, catechol reached higher concentration than hydroquinone. There were some high molecular weight compounds in MS spectrum founded other than catechol and hydroquinone, i.e. 2-phenoxy-phenol, 1,4-benzenedicarboxylic acid, (1,1-dimethylethyl)-2-methoxy phenol, 2,6-bis(1,1-

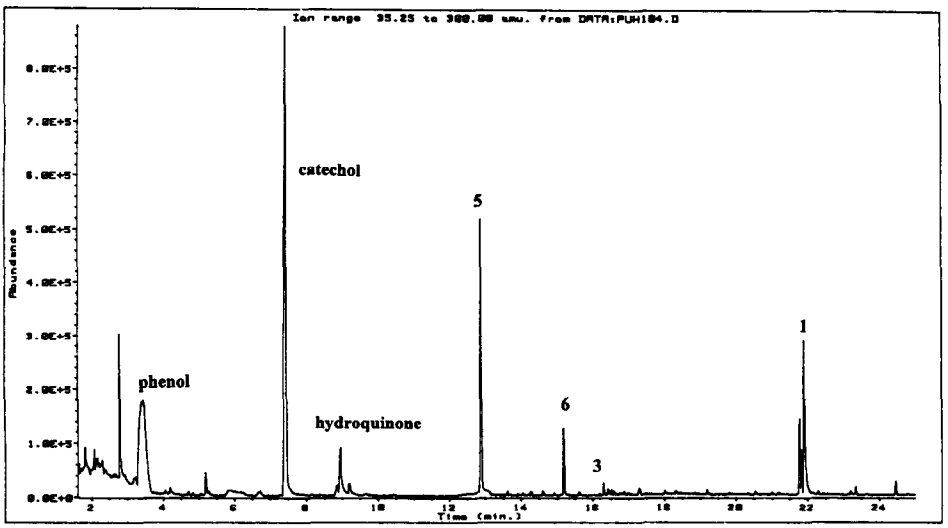

Fig. 7. GC/MS total ion chromatograph for phenol decomposition by UV/hydrogen peroxide system after 104 min of reaction. Intermediate marked No. 1 is α-methoxy-α-methyl-benzeneethanol; compounds around No. 3 are isomers of 2-phenoxy-phenol; No. 5 is 3-methoxy-2,4,5-trimethyl-phenol; No. 6 is 2-(2-butenyl)-4-hydroxy-3-methyl-2-cyclopenten-1-one.

dimethylethyl)-naphthalene, 2,3-dihydro-1,4-benzodioxin-2-methanol, 1,1′-biphenyl-2,2′-diol, as shown in Fig. 7. Experimental data were plotted in Fig. 8. The plot shows agreement between experimental data and model prediction for the UV/hydrogen peroxide oxidation of phenol. From these data, the five reaction rate constants were evaluated and listed in Table 4.

4.5. Photolytic ozonation of phenol

The proposed mechanisms of photolytic ozonation of phenol were also presented in Fig. 4 which combines ozonation and hydroxyl free radical reaction with phenol. From GC/MS analysis (Fig. 9), we proposed that the reaction pathway of photolytic ozonation was very similar to the ozonation of phenol. However, some high molecular weight compounds but at very low concentrations were found as intermediates. These compounds were 2-phenoxy-phenol, 1,1′-biphenyl-2,2′-diol, diisooctyl ester, 1,2-benzenedicarboxylic acid, and dicyclohexyl ester of 1,2-benenedicarboxylic acid. The reason why high molecular weight compounds formed were hydroxyl free radical conversion of phenol to a phenolic radical, then the phenolic radical reacted with phenol to produce those compounds. Experimental data on the concentration change of phenol, intermediate, hydroquinone and catechol, and the pH versus time are plotted in Fig. 10. Results of calculated rate constants of each pathway were tabulated in Table 4.

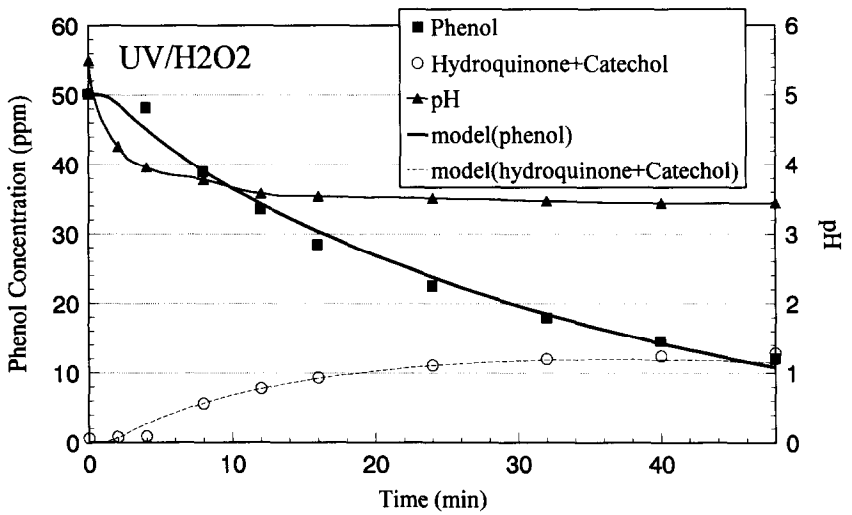

Fig. 8. Experimental data and model fitting for phenol decomposition by UV/hydrogen peroxide system. Initial phenol concentration is 50.1 mg/l and initial hydrogen peroxide concentration is 7.08 mg mol/l.

Table 4
Elementary rate constants obtained from computer modeling

Reaction[a]	Rate constants (l/mol s)
Phenol + O_3 → hydroquinone, catechol	1.30×10^3
Hydroquinone, catechol + O_3 → B_3	4.04×10^3
B_3 + O_3 → product	1.25×10^3
Phenol + $OH^{\cdot}$ → hydroquinone + catechol	4.50×10^9
Phenol + $OH^{\cdot}$ → ph· (phenolic radical)	2.10×10^9
ph· + phenol → high molecular weight compounds	1.75×10^4
Hydroquinone, catechol + $OH^{\cdot}$ → organic acid	7.00×10^9
Phenol + $HO_2^{\cdot}$ → products	8.55×10^4

[a] B_3 denotes organic acids produced by ozonation, which reacts with ozone.

4.6. Computer obtained rate constants

The phenol degradation kinetics in ozonation, UV/O_3 UV/H_2O_2 systems has been introduced in the "Proposed Model" section of this paper. The reaction pathways were suggested by the intermediates and final product analysis by GC/MS. The modeling mechanism considered both the data from the kinetics and pathways. By using an ODE solver and Rosenbrock Hillclimb optimization algorithm to fit experimental data with mass balance equations, the reaction rate constants could be solved

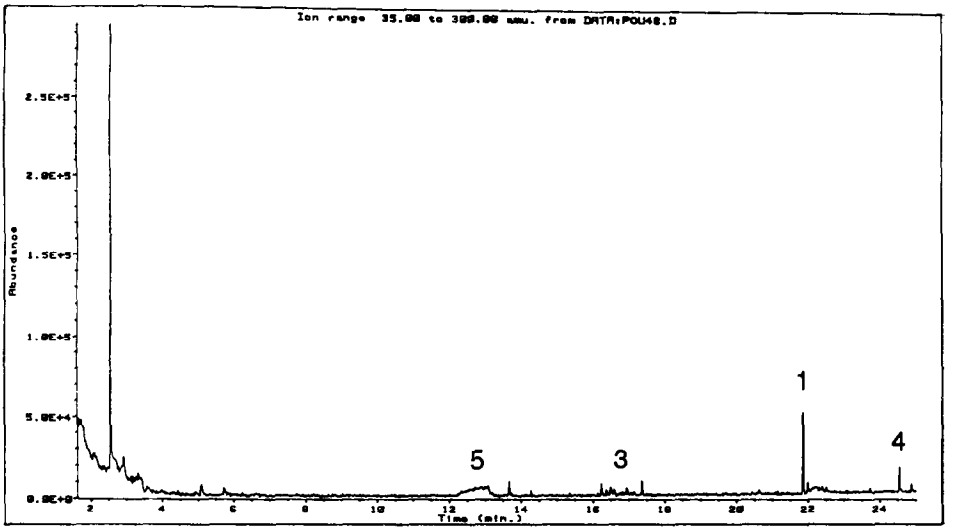

Fig. 9. GC/MS total ion chromatograph for phenol decomposition by UV/ozone after 24 min of reaction. Intermediate marked No. 4 is 1,2-benzenedicarboxylic acid dicyclohexyl ester; the rest of the intermediates is similar to UV/hydrogen peroxide reaction and ozonation.

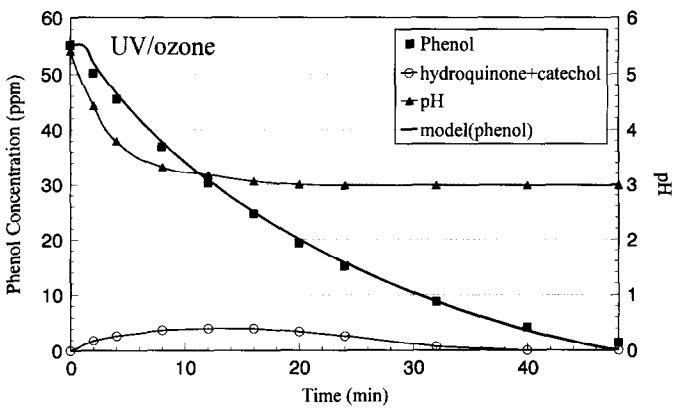

Fig. 10. Experimental data and model fitting for phenol decomposition by UV/ozone system. Initial phenol concentration is 55.6 ppm, and oxygen flow rate to the ozone generator was 6.0 l/min of oxygen.

by VAX system. The computed rate constants which were consistent with the literature data are listed in Table 4.

5. Conclusions

In our studies of the decomposition of phenol in three systems, i.e. ozonation, UV/ozone, and UV/hydrogen peroxide, we incorporated the following three indepen-

dent sources of information into a kinetic model: first, the well-estabilished fundamental free radical reaction mechanisms and their published values of rate constants; second, the identification of intermediates of these three reaction systems via GC/MS; and third, the experimental data of phenol decomposition in a batch reactor. The results showed that the kinetic model can accurately predict the concentration profile of phenol and intermediates in each system. The reaction rate constants of each pathway could be evaluated simultaneously. We believe that our model and obtained reaction rate constants are accurate to be used to design or scale-up UV/ozone and UV/hydrogen peroxide reactors in the future.

6. Nomenclature

I	light intensity at any point p ($\mu W/cm^2$)
I_0	light intensity at lamp wall ($\mu W/cm^2$)
E	monochromatic absorbance of solution (cm^{-1})
m	ratio of average light intensity to the light intensity of lamp wall
k_{10}, k_{11}, k_{14}, k_{15}, k_{16}, k_8, k_4, k_5, k_1	elementory reaction rate constant (l/mol s)
$K_{LO_3}a$	ozone mass transfer coefficient (s^{-1})
C_{SO_3}	saturated aqueous ozone concentration (M)
$k_{IO_3}I$, $k_{IH_2O_2}I$, $k_{IH_2O_2}I_0$	photodecomposition rate constant for ozone and hydrogen peroxide (s^{-1})
C_{O_3}, $C_{H_2O_2}$, $C_{OH\cdot}$, $C_{HO_2\cdot}$	aqueous concentration of ozone, hydrogen peroxide, OH and HO_2 radicals (M)

Acknowledgements

The authors gratefully acknowledge funding from the US EPA Northeast Hazardous Substance Management and Research Center and the generous donation of UV lamp and accessories from Canard-Honovia Inc., Newark, New Jersey.

References

[1] M.C. Goronszy, W.W. Eckenfelder and E. Froelich, Waste water – A guide to industrial pretreatment, Chem. Eng., 7 (1992) 78–83.

[2] P.W. Smith, Enhanced oxidation destroys dimethylnitrosamine, Water Environ. Technol., 10 (1992) 67–69.

[3] D.W. Sundstrom, H.E. Klei, T.A. Nalette, D.J. Reidy and B.A. Weir, Destruction of halogenated aliphatics by ultraviolet catalyzed oxidation with hydrogen peroxide, Hazard. Waste Hazard. Mater., 3 (1986) 101–110.

[4] D.W. Sundstrom, B.A. Weir and H.E. Klei, Destruction of aromatic pollutants by UV light catalyzed oxidation with hydrogen peroxide, Environ. Progress, 8 (1989) 6–11.

[5] B.A. Weir, D.W. Sundstrom and H.E. Klei, Destruction of benzene by ultraviolet light-catalyzed oxidation with hydrogen peroxide, Hazard. Waste Hazard. Mater., 4 (1987) 165–176.
[6] P.C. Ho, Photooxidation of 2,4-dinitrotoluene in aqueous solution in the presence of hydrogen peroxide, Environ. Sci. Technol., 20 (1986) 260–267.
[7] N. Lewis, K. Topudurti, G. Welshans and R. Foster, Removal of organics in water using hydrogen peroxide in presence of ultraviolet light, Water Res., 40 (1990) 540–547.
[8] C. Prat, M. Vicente and S. Esplugas, Treatment of bleaching waters in the paper industry by hydrogen peroxide and ultraviolet radiation, Water Res., 22 (1988) 663–668.
[9] J. Shearman, The clean oxidizer, Chem. Eng., 7 (1992) 55–57.
[10] P. Stryker and P. Lone, Cutting Chemical Wastes, Inform. New York, 1985, pp. 44–130.
[11] M. Trillas, M. Pujol and X. Domenech, Phenol photodegradation over titanium dioxide, J. Chem. Tech. Biotechnol., 55 (1992) 85–90.
[12] T.Y. Wei and C.C. Wan, Heterogeneous photocatalytic oxidation of phenol with titanium dioxide powders, Ind. Eng. Chem. Res., 30 (1991) 1293–1300.
[13] N. Al-Hayek and M. Dore, Oxidation of phenols in water by hydrogen peroxide on alumine supported iron, Water Res., 24 (1990) 973–982.
[14] T.D. Thornton and P.E. Savage, Kinetics of phenol oxidation in supercritical water, A.I.Ch.E. J., 38 (1992) 321–327.
[15] T.D. Thornton and P.E. Savage, Phenol oxidation pathways in supercritical water, Ind. Eng. Chem. Res. 31 (1992) 2451–2456.
[16] T.D. Thornton, D.E. Ladue and P.E. Savage, Phenol oxidation in supercritical water: Formation of dibenzofuran, dibenzo-*p*-dioxin, and related compounds, Environ. Sci. Technol., 25 (1991) 1507–1510.
[17] R.J. Field, N.V. Raghavan and J.G. Brummer, A pulse radiolysis investigation of the reactions of BrO_2 with $Fe(CN)_6^{4-}$, Mn^{2+}, phenoxide, and phenol, J. Phys. Chem., 86 (1982) 2443–2449.
[18] B.H.J. Bielski, D.E. Cabelli, R.L. Arudi and A.B. Ross, Reaction of HO_2/O_2^- radicals in aqueous solution, J. Phys. Chem. Ref. Data, 14 (1985) 1041–1100.
[19] G.V. Buxton, W. Greenstock, P. Helman and A.B. Ross, Critical review of rate constants for reaction of hydrated electrons, hydrogen atom and hydroxyl radicals in aqueous solution, J. Phys. Chem. Ref. Data, 17 (1988) 513–886.
[20] P. Neta, R.E. Huie and A.B. Ross, Rate constants for reaction of inorganic radicals in aqueous solution, J. Phys. Chem. Ref. Data, 17 (1988) 1027–1284.
[21] W. Masschelein, M. Denis and R. Lendent, Spectrophotometric determination of residual hydrogen peroxide, Water Sewage Works, 8 (1977) 69–72.
[22] H. Shechter, Spectrophotometric method for determination of ozone in aqueous solutions, Water Res., 7 (1973) 729–739.